PROCEEDINGS OF SCIENCE

$K \to \pi\nu\bar{\nu}$ from NA62 and KOTO

Angela Romano[*†]
University of Birmingham
E-mail: angela.romano@cern.ch

A review of the present experimental status of the $K \to \pi\nu\bar{\nu}$ decays is given. The NA62 experiment at CERN is designed to measure the branching ratio (BR) of the $K^+ \to \pi^+\nu\bar{\nu}$ decay with a novel kaon decay-in-flight technique. One candidate event, compatible with the Standard Model (SM) prediction, has been observed from a sample of 1.2×10^{11} decays collected by NA62 in 2016. A larger data sample will be available to NA62 by the end of 2018 for the measurement of BR($K^+ \to \pi^+\nu\bar{\nu}$). The aim of the KOTO experiment at JPARC is to study the $K_L \to \pi^0\nu\bar{\nu}$ decay using a kaon decay-in-flight technique, with a much lower momentum than NA62. The data collected by KOTO and the analysis strategy are presented. Improvements on both hardware and analysis levels necessary to reach the SM sensitivity for $K_L \to \pi^0\nu\bar{\nu}$ are outlined.

The International Conference on B-Physics at Frontier Machines - BEAUTY2018
6-11 May, 2018
La Biodola, Elba Island, Italy

[*]Speaker.
[†]on behalf of NA62 and KOTO Collaborations.

© Copyright owned by the author(s) under the terms of the Creative Commons Attribution-NonCommercial-NoDerivatives 4.0 International License (CC BY-NC-ND 4.0).

PoS(BEAUTY2018)028

1. Introduction

The decays $K \to \pi\nu\bar{\nu}$ are Flavour Changing Neutral Current (FCNC) processes particularly interesting to study the physics of flavour. In the Standard Model (SM) these decays are extremely rare due to quadratic GIM mechanism and strong Cabibbo suppression; they can only proceed through Z penguin and W box (one-loop) diagrams. The decay amplitudes are dominated by short-distance dynamics and their rate can be computed with extremely high precision. The leading SM contribution to the matrix element is generated by top quark loops and can be computed with negligible theoretical uncertainty. In case of $K^+ \to \pi^+\nu\bar{\nu}$ decay there is a small sub-leading contribution from charm quark computed at NNLO order [1]. The hadronic matrix element can be extracted from the well measured $K^+ \to e^+\pi^0\nu_e$ decays rate [2]. The SM current predictions for the branching ratios using elements of the Cabibbo-Kobayashi-Maskawa (CKM) matrix extracted from tree-level processes are [3, 4]:

$$BR(K^+ \to \pi^+\nu\bar{\nu}) = (8.4 \pm 1.0) \times 10^{-11} \qquad BR(K_L \to \pi^0\nu\bar{\nu}) = (3.4 \pm 0.6) \times 10^{-11}$$

with uncertanties dominated by the knowledge of the external inputs. The $K \to \pi\nu\bar{\nu}$ decays are sensitive to physics beyond the SM, with large deviations expected in several scenarios [5]:

- tree-level FCNC mediated by heavy gauge boson (Z') [6], for which the combined measurement of BR($K^+ \to \pi^+\nu\bar{\nu}$) and BR($K_L \to \pi^0\nu\bar{\nu}$) should show specific correlations;
- recent models with Lepton Flavour Universality (LFU) violation [7], in which the anomalies observed in semileptonic B meson decays could be linked to BR($K^+ \to \pi^+\nu\bar{\nu}$).

The experimental status of $K^+ \to \pi^+\nu\bar{\nu}$ relies on a combined measurement obtained by E787-E949 collaborations at Brookhaven National Laboratory [8]. The result obtained with a kaon decay-at-rest technique is: BR($K^+ \to \pi^+\nu\bar{\nu}$) $= (17.3^{+11.5}_{-10.5}) \times 10^{-11}$, consistent with the SM expectation with a large statistical uncertainty. An upper limit at 90% C.L BR($K_L \to \pi^0\nu\bar{\nu}$) $< 2.6 \times 10^{-8}$ has been set by the E391a experiment [9].

2. The NA62 experiment at CERN

The NA62 experiment [10] at the CERN SPS is a fixed target detector designed for the study of rare kaon decays. It represents the current kaon physics programme at CERN and offers a complementary approach, with respect to the Large Hadron Collider high energy frontier, to probe new physics at short distances, corresponding to energy scales up to 100 TeV. The NA62 primary goal is to measure BR($K^+ \to \pi^+\nu\bar{\nu}$) with a 10% precision, using a novel technique with kaon decays in flight. A background rejection at the level of 10^{12} is required in order to keep the signal over background ratio at about 10 and to match the theoretical predictions.

In NA62 the most important background processes to $K^+ \to \pi^+\nu\bar{\nu}$ events are the main K^+ decay modes (see Tab. 1), with rates up to 10^{10} times larger than the one expected for the signal. The kinematics of the $K^+ \to \pi^+\nu\bar{\nu}$ decay can be fully described by the squared missing mass variable $m^2_{miss} = (P_K - P_\pi)^2$, where P_K is the kaon candidate 4-momentum and P_π is the pion candidate 4-momentum. The theoretical distributions of m^2_{miss} for signal and backgrounds from the main K^+

PoS(BEAUTY2018)028

Process	Branching Ratio	Rejection Technique
$K^+ \to \mu^+\nu_\mu$	63%	Kinematics + μ-PID
$K^+ \to \pi^+\pi^0$	21%	Kinematics + γ-Veto
$K^+ \to \pi^+\pi^+\pi^-$	6%	Kinematics + π^--Veto
$K^+ \to e^+\pi^0\nu_e$	5%	e-PID + γ-Veto
$K^+ \to \mu^+\pi^0\nu_\mu$	3%	μ-PID + γ-Veto

Table 1: Dominant kaon decays, their branching ratios and corresponding rejection techniques. The first three channels are kinematically constrained, while the last two channels are kinematically non-constrained.

decay channels are shown in Fig 1, backgrounds are normalised according to their branching ratio and the signal is multiplied by a factor 10^{10}. Due to the $K^+ \to \pi^+\pi^0$ kinematics, which produces a spike in the middle of the signal region, two separate kinematic regions (R1, R2) are defined for the $K^+ \to \pi^+\nu\bar{\nu}$ acceptance: R1 positioned above the $K^+ \to \mu^+\nu_\mu$ contribution and below the $K^+ \to \pi^+\pi^0$ peak, R2 is above the $K^+ \to \pi^+\pi^0$ contribution but below the $K^+ \to \pi^+\pi^+\pi^-$ threshold. The background rejection relies on kinematics, through the definition of the π^+ momentum range (15-35) GeV/c and the two signal regions (R1, R2). To guarantee a background rejection at the required level of 10^{12}, kinematic constraints must be used in conjunction with particle identification (PID) and veto systems, as shown in the third column of Tab. 1.

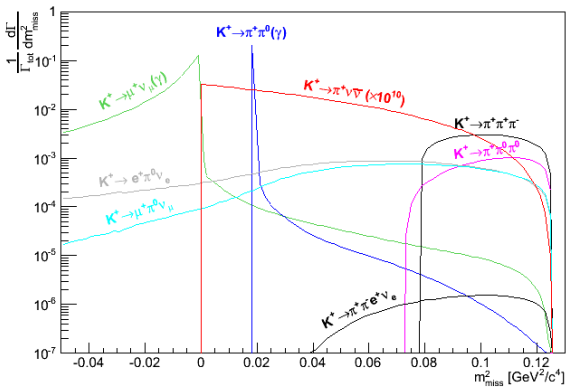

Figure 1: Distributions of m^2_{miss} for signal and backgrounds from the main K^+ decay channels, the backgrounds are normalised according to their branching ratio and the signal is multiplied by a factor 10^{10}.

2.1 The beam and detector

NA62 uses a high intensity particle beam with kaon decay-in-flight technique. A secondary unseparated hadron beam of central momentum (75±0.8) GeV/c is produced from SPS primary protons at 400 GeV/c directed on a beryllium target. The total particle rate is about 750 MHz and the main beam components correspond to ∼ 70% of π^+, ∼ 6% of K^+ and ∼ 24% of protons. About 10% of K^+ decays in a 60 m fiducial volume (FV). The schematic layout of the NA62 experiment comprising the target, secondary beam line, FV and detectors is shown in Fig. 2. The FV is contained in a large vacuum cylindrical tank kept at 10^{-6} mbar pressure, to minimise the multiple scattering of the decay products and the number of interactions of the beam with the residual gas.

PoS(BEAUTY2018)028

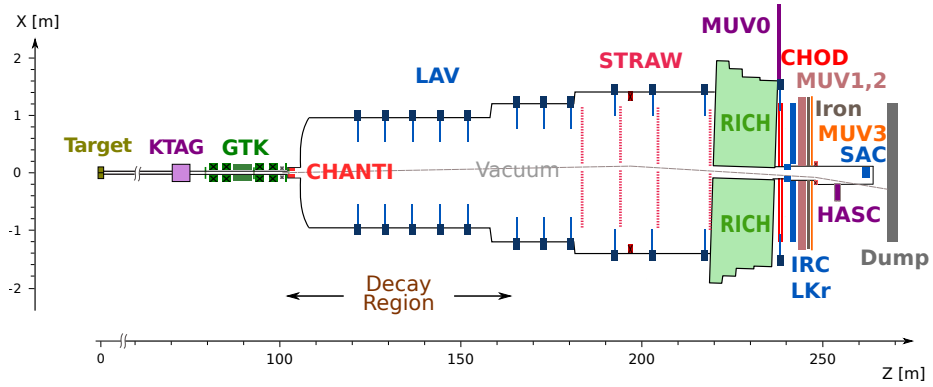

Figure 2: Schematic layout of the NA62 experiment in the *xz* plane.

The NA62 tracking system is composed by three stations of silicon micro-pixel GigaTracKer (GTK) beam spectrometer and four straw chambers spectrometer (STRAW) responsible for the detection and tracking of particles upstream and downstream the FV, respectively. The NA62 PID strategy relies on a Cherenkov differential counter (KTAG) for the positive identification of kaons upstream the FV, a Ring Imaging Cherenkov (RICH) detector for π/μ separation and timing, a liquid Kripton (LKr) electromagnetic calorimeter and hadronic calorimeters (MUV1,2) for $\pi/\mu/e$ separation. The NA62 photon veto system is composed by several detectors covering different photon emission angle regions: LKr, intermediate (IRC) and small angle (SAC) calorimeters responsible for the rejection of photons emitted in the forward region (up to 15 mrad), 12 stations of large angle vetoes (LAV), distributed over the whole length of the decay tank, for photons emitted at large angle (15-50 mrad). The veto system also comprises plastic scintillators (MUV0, MUV3) to suppress muons. Detector redundancy is necessary to reach a background rejection at the required level of 10^{12}, that includes charged hodoscopes (CHODs), upstream anti-counter (CHANTI) to veto charged particle produced from interactions in the third station of GTK and a hadronic calorimeter (HASC) to detect pions from kaon decays travelling along the beam pipe. A detailed descriptions of the NA62 apparatus and its performances measured in 2015 can be found in [11].

3. The NA62 $K^+ \to \pi^+\nu\bar{\nu}$ analysis

The analysis of a data sample corresponding to $N_K = 1.21(2) \times 10^{11}$ kaon decays collected by NA62 in 2016 at CERN SPS is presented here. The first step of the signal selection is the requirement of K^+ decays in the fiducial region with single track topology (see Fig. 3). For these events the π^+ mass is assigned to the downstream track and the distribution of the reconstructed m^2_{miss} as a function of the downstream track momentum is shown. The kinematics of the main K^+ decays ($K^+ \to \pi^+\pi^0$, $K^+ \to \mu^+\nu_\mu$ and $K^+ \to \pi^+\pi^+\pi^-$) is clearly visible. In particular the negative distribution from $K^+ \to \mu^+\nu_\mu$, as the π^+ mass is assigned to the downstream track; the peak from $K^+ \to \pi^+\pi^0$ (from the π^0 invariant mass) and the upper bound from $K^+ \to \pi^+\pi^+\pi^-$ decays. Against these decays two signal regions are defined for the analysis (R1, R2), which are drawn in Fig. 3 (red box) for reference.

PoS(BEAUTY2018)028

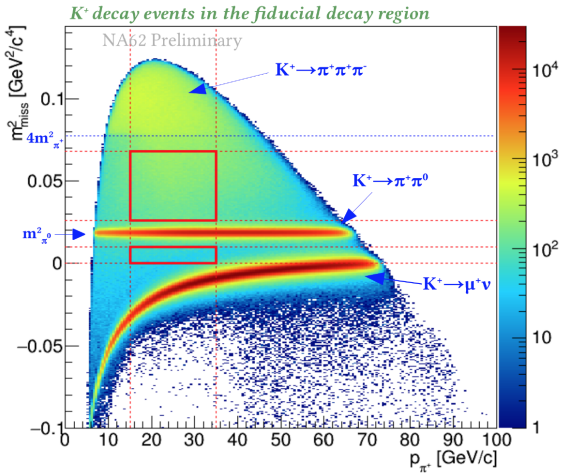

Figure 3: Distribution of m^2_{miss} as a function of the track momentum, for K^+ decay events with single track topology and selected on minimum bias data. The main K^+ decays ($K^+ \to \pi^+\pi^0$, $K^+ \to \mu^+\nu_\mu$ and $K^+ \to \pi^+\pi^+\pi^-$) are clearly visible. The π^+ mass is assigned to the pion track, thus deforming the kinematics of $K^+ \to \mu^+\nu_\mu$. The two kinematic signal regions defined for the analysis (red box) are drawn for reference.

The m^2_{miss} resolution achieved for the signal is $\sigma(m^2_{miss}) \sim 10^{-3}\,\mathrm{GeV}^2/c^4$ and meet the detector design. Upper and lower limits of the two signal regions are chosen about $10 \times \sigma(m^2_{miss})$ away from the m^2_{miss} distributions of $K^+ \to \pi^+\pi^0$, $K^+ \to \mu^+\nu_\mu$ and $K^+ \to \pi^+\pi^+\pi^-$, in order to minimize background contributions from gaussian tails. The residual backgrounds entering the signal regions are due to non-gaussian resolution and radiative tails, or kaon decays with non-constrained kinematics ($K^+ \to e^+\pi^0\nu_e$, $K^+ \to \mu^+\pi^0\nu_\mu$ and $K^+ \to \pi^+\pi^-e^+\nu_e$ with neutrinos in the final state), or upstream background from early K^+ decays (upstream of the third GTK station) and inelastic beam-detector interactions.

The signal selection then proceeds through the π^+ identification, photon and multi-track rejections. The π^+ tracks are identified combining the information from the RICH detector and the calorimeters (LKr, MUV1-2-3); a muon suppression of $\sim 10^8$ and a pion efficiency of 64% are measured with control samples of $K^+ \to \pi^+\pi^0$ and $K^+ \to \mu^+\nu_\mu$ kinematically selected with minimum bias data. Events with in-time extra energy depositions in the LKr are rejected if the corresponding clusters are more than 10 cm away from the impact position of the π^+ on the LKr. Events with hits in either the LAV, SAV, IRC or HASC in time with the π^+ are rejected. Combining downstream information from STRAW, CHODs and LKr, events with extra charged particles in the final state not reconstructed in the spectrometer or with photons interacting in the material before reaching LKr, LAV and SAV are also rejected. A $\pi^0 \to \gamma\gamma$ suppression of 3×10^8 is measured with minimum bias as well as $K^+ \to \pi^+\nu\bar{\nu}$-triggered data before and after the photon rejection.

The kinematic suppression factor is measured on data with control samples of $K^+ \to \pi^+\pi^0$ and $K^+ \to \mu^+\nu_\mu$ selected using only the information from calorimeters. The fraction of residual events entering the signal regions (due to kinematic tails) is found to be: 3×10^{-4} for $K^+ \to \mu^+\nu_\mu$ and 1×10^{-3} for $K^+ \to \pi^+\pi^0$. The kinematic suppression factor is used for the background estimations.

PoS(BEAUTY2018)028

3.1 Results

A sample of $K^+ \to \pi^+\pi^0$ selected on minimum bias data using similar $K^+ \to \pi^+\nu\bar{\nu}$ criteria is used for normalisation. The measured single event sensitivity is $SES = (3.15 \pm 0.01_{stat} \pm 0.24_{syst}) \times 10^{-10}$. The large systematics is dominated by random veto losses induced by the $\pi^0 \to \gamma\gamma$ rejection, which will be improved in the future. The $K^+ \to \pi^+\nu\bar{\nu}$ acceptance is computed with MC at the end of the signal event selection and region definitions; the total acceptance is 4% and is distributed as 1% in R1 and 3% in R2. The backgrounds to $K^+ \to \pi^+\nu\bar{\nu}$ are studied with data driven methods in background regions and extrapolated to the signal and control regions. and corrected for kinematic and radiative tails. The number of expected signal and background events in signal regions are reported in Tab. 2. The upstream background estimate is statistically limited with the 2016 data set. This reflects the large uncertainty dominating the overall background estimation.

Process	Expected events in R1 + R2
$K^+ \to \pi^+\nu\bar{\nu}$ (SM)	$0.267 \pm 0.001_{stat} \pm 0.020_{syst} \pm 0.032_{ext}$
$K^+ \to \pi^+\pi^0(\gamma)IB$	$0.064 \pm 0.007_{stat} \pm 0.006_{syst}$
$K^+ \to \mu^+\nu_\mu(\gamma)IB$	$0.020 \pm 0.003_{stat} \pm 0.003_{syst}$
$K^+ \to \pi^+\pi^-e^+\nu_e$	$0.018^{+0.024}_{-0.017}\|_{stat} \pm 0.009_{syst}$
$K^+ \to \pi^+\pi^+\pi^-$	$0.002 \pm 0.001_{stat} \pm 0.002_{syst}$
Upstream background	$0.050^{+0.090}_{-0.030}\|_{stat}$
Total background	$0.15 \pm 0.09_{stat} \pm 0.01_{syst}$

Table 2: Expected number of signal and background events in signal regions (R1 + R2), after applying the complete $K^+ \to \pi^+\nu\bar{\nu}$ analysis on the 2016 NA62 data set.

One event is found in region R2 after un-bliding the signal regions (Fig. 4, left). The $K^+ \to \pi^+\nu\bar{\nu}$ candidate event has $P_{\pi^+} = 15.3$ GeV$/c$ momentum and is perfectly consistent with a π^+ ring in the RICH detector (Fig. 4, right).

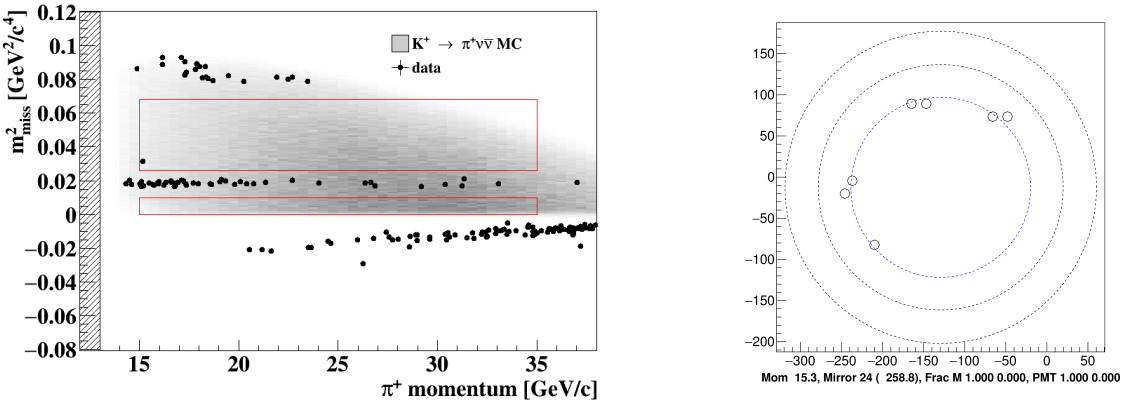

Figure 4: Left: m^2_{miss} as a function of the π^+ momentum for data passing the $K^+ \to \pi^+\nu\bar{\nu}$ selection, except for cuts on m^2_{miss} and P_{π^+}. The grey area corresponds to the distributions of $K^+ \to \pi^+\nu\bar{\nu}$ MC events. The signal regions (red box) are drawn. The un-blinding of the signal regions reveals one event observed in R2. Right: RICH display showing the hits associated to the track for the event observed in R2. The three circles illustrate the positron, muon and pion hypothesis, showing a perfect agreement with the innermost ring corresponding to the pion hypothesis.

PoS(BEAUTY2018)028

Assuming that the observed event is background, a 95% CL upper limit is set:

$$BR(K^+ \to \pi^+\nu\bar{\nu}) < 14 \times 10^{-10}.$$

For comparison, if the candidate is assumed as to be signal, the branching ratio at 68% CL is:

$$BR(K^+ \to \pi^+\nu\bar{\nu}) = 28^{+44}_{-23} \times 10^{-11}.$$

This certainly shows that the NA62 novel decay-in-flight technique works and the experiment is ready to precisely measure BR($K^+ \to \pi^+\nu\bar{\nu}$). In 2017 a four-month data taking dedicated to $K^+ \to \pi^+\nu\bar{\nu}$ has taken place and the experiment is currently running (in 2018) for a seven-month run. The $K^+ \to \pi^+\nu\bar{\nu}$ analysis on 2017 data is ongoing; improvements at hardware and analysis levels are foreseen to reduce the background and improve the signal efficiency. By the end of 2018, considering the whole data set, NA62 should have observed at least 20 SM $K^+ \to \pi^+\nu\bar{\nu}$ events.

4. The KOTO experiment at J-PARC

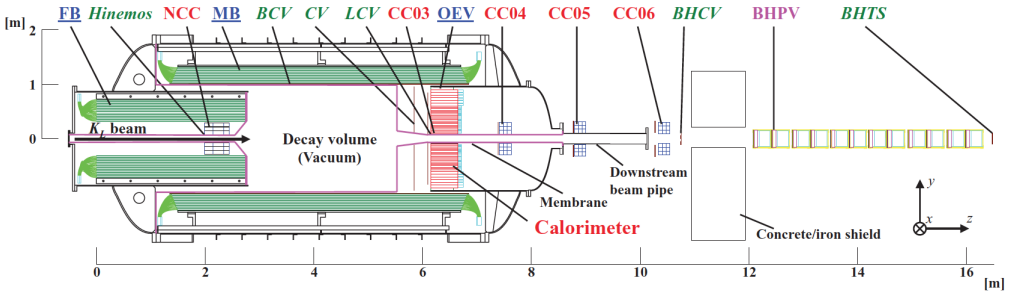

Figure 5: Schematic layout of the KOTO experiment in the *xz* plane.

The KOTO experiment [12] at J-PARC is a fixed target detector aiming to observe few SM $K_L \to \pi^0\nu\bar{\nu}$. A schematic view of the KOTO detector is shown in Fig. 5. Primary protons at 30 GeV/c are extracted from the Main Ring accelerator and directed onto a 66 mm-long gold target. K_L with a peak momentum of 1.4 GeV/c are produced at an angle of 16 degrees with respect to the proton beam; the neutral beam also contained neutrons and photons. A halo of neutrons originated from scattering inside the collimators on the beam line and travelling outside the nominal beam solid angle is present. The K_L decay volume is 3 m-long and is hosted inside the detector along the beam direction. To suppress π^0 produced in the interactions of beam neutrons with residual gas the decay volume is kept at 5×10^{-7} mbar. The main subsystem of the KOTO detector is the electromagnetic calorimeter made of un-doped CsI crystals, which is responsible for the detection of the $\pi^0 \to \gamma\gamma$ decay in the final state of the signal. Other subsystems in the KOTO detector are veto counters, which ensure that no other detectable particles are emitted in the K_L decay; lead-scintillator sandwich counters, covering the gaps between the cylinder and the crystals of the calorimeter. The outside region of the decay volume is surrounded by the Main Barrel (MB), which is a sandwich-type shower counter with lead and plastic scintillator sheets responsible for

PoS(BEAUTY2018)028

the detection of extra particles from $K_L \to \pi^0\pi^0$ and $K_L \to \pi^0\pi^0\pi^0$. The upstream end of the decay region is covered by the Front Barrel (FB) and the Neutron Collar Counter (NCC). The former is a lead-scintillator sandwich counter and the latter is made of CsI crystals. Both these veto counters are responsible for the detection of photons from K_L decays upstream the decay region.

5. The KOTO $K_L \to \pi^0\nu\bar{\nu}$ analysis

The $K_L \to \pi^0\nu\bar{\nu}$ decay signature is given by two photons from a π^0 decay, with no other particles detected. Events with two photons in the final state are selected in the KOTO analysis for π^0 reconstruction. Assuming that the $\pi^0 \to \gamma\gamma$ decay occurred on the beam axis, then the decay vertex position (Z_{vtx}) along the beam axis is calculated. The CsI calorimeter information and Z_{vtx} are used to determine the transverse momentum (P_T) and π^0 decay time. The signal region for $K_L \to \pi^0\nu\bar{\nu}$ is defined by the Z_{vtx} of the reconstructed π^0 and P_T as it can see in Fig. 5.

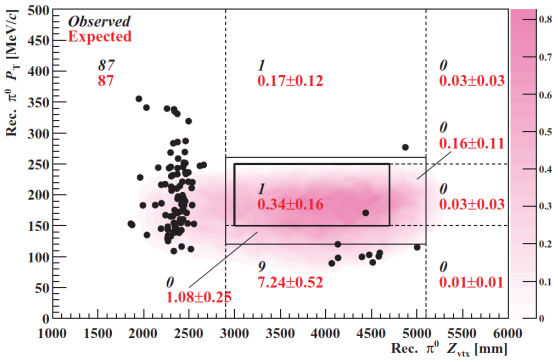

Figure 6: Distribution of π^0 P_T versus Z_{vtx} for data passing the $K_L \to \pi^0\nu\bar{\nu}$ selection, with all cuts imposed. The black dots represent the data, while the contour corresponds to the distribution of $K^+ \to \pi^+\nu\bar{\nu}$ MC events. The signal regions (thick solid line) are drawn. The black italic (red regular) numbers indicate the numbers of observed events (expected background events) for the regions divided by solid and dashed lines.

The analysis of a data sample corresponding to $\sim 2.3 \times 10^{11}$ K_L decays collected by KOTO in 2013 is presented here. The achieved $SES = 1.3 \times 10^{-8}$ is comparable to the final sensitivity of the E391a experiment. One event is observed, as shown in Fig. 5, consistent with the expected number of background events 0.34 ± 0.16 in the signal region. This leads to the following upper limit $BR(K_L \to \pi^0\nu\bar{\nu}) < 5.1 \times 10^{-8}$ at 90% C.L. [13]. The result is limited by background from neutrons and set the level of KOTO sensitivity, showing path for improvements. Backgrounds to $K_L \to \pi^0\nu\bar{\nu}$ are categorised mainly into two types: K_L and neutron backgrounds. The $K_L \to \pi^0\pi^0$ decay is the major K_L background source as there are only two extra photons that can be detected by veto counters. Neutron backgrounds are mainly caused by halo neutrons: one type comes from halo neutrons interacting with the NCC detector material in the upstream end of the decay volume; another type is due to halo neutrons directly hitting the calorimeter.

After 2013 KOTO has re-designed the entrance region and instrumented the beam pipe to reduce the backgrounds to $K_L \to \pi^0\nu\bar{\nu}$. Improvements at the analysis level are also achieved with new methods to discriminate photons from neutrons, based on shower cluster shape and waveform

PoS(BEAUTY2018)028

of hit crystals [14]. KOTO collected a data set in 2015, which is roughly 20 times larger than the 2013 one. A subset of KOTO 2015 statistics, comparable in size to the 2013 data set, is under analysis. Preliminary results show an improved background rejection allowing for a signal acceptance larger by 40% with respect to the one defined for the analysis of 2013 data. The SES achieved with this subset is $\sim 5.9 \times 10^{-9}$. The prospects for the full data sample collected in 2015-2016 are a SES $< 10^{-9}$. The preliminary analysis of 2015 data proves that the major background observed in the 2013 data set is well suppressed and better controlled. Nevertheless the goal of KOTO is to reach the SM SES for $K_L \to \pi^0\nu\bar{\nu}$ and the preliminary results for the projected background to the SM SES show that the current background rejection power is not enough and more upgrades of the KOTO detector are needed. The list of necessary interventions can be found in details here [14]; the timeline for some more complex actions (like upgrading the JPARC power line) is extending up to 2019. With the detector upgrade KOTO should reach the SM SES for $K_L \to \pi^0\nu\bar{\nu}$ around 2021, just at the same time as NA62 should resume the data taking to complete the measurement.

6. Conclusions

The SM sensitivity for $K^+ \to \pi^+\nu\bar{\nu}$ has been reached with the completion of NA62 2016 data analysis. The results achieved on 2016 data have proved that the kaon-in-flight technique works. The analysis of NA62 2017-2018 data will establish the observation of the $K^+ \to \pi^+\nu\bar{\nu}$ decay. KOTO should reach a sensitivity for $K_L \to \pi^0\nu\bar{\nu}$ of $< 10^{-9}$ soon; while the SM sensitivity is expected with the detector upgrade by 2021. At that point combined constraints from both collaborations should shed some important light on the correlations predicted by several SM extensions.

References

[1] A. J. Buras, M. Gorbahn, U. Haisch, U. Nierste *JHEP* **0611** (2006) 002.

[2] C. Amsler *et al.*, *Phys. Lett.* **B 667** (2008) 1.

[3] A. J. Buras, D. Buttazzo, K. Girrbach-Noe, R. Knegjens *JHEP* **1511** (2015) 033.

[4] J. Brod, M. Gorbahn, E. Stammou *Phys. Rev.* **D 83** (2011) 034030.

[5] M. Blanke, A. J. Buras, S. Recksiegel *Eur. Phys. J* **C 76** (2016) no.4 182.

[6] A. J. Buras, D. Buttazzo, R. Knegjens *JHEP* **1511** (2015) 166.

[7] G. Isidori, M. Bordone, D. Buttazzo, J. Monnard *Eur. Phys. J* **C 77** (2017) 618.

[8] A. V. Artamonov *et al.*, [E949 Collaboration] *Phys. Rev.* **D 79** (2009) 092004.

[9] J. K. Ahn *et al.*, [E391a Collaboration] *Phys. Rev.* **D 81** (2010) 072004.

[10] G. Anelli *et al.*, *Proposal to measure the rare decay $K^+ \to \pi^+\nu\bar{\nu}$ at the CERN SPS*, CERN-SPSC-2005-013 (2005).

[11] E. Cortina *et al.*, [NA62 Collaboration] *JINST* **12** (2017) P05025.

[12] T. Yamanaka *et al.*, [KOTO Collaboration] *PTEP* **2012** (2012) 02B006.

[13] J. K. Ahn *et al.*, [KOTO Collaboration] *PTEP* **2017** (2017) no.2 021C01.

[14] K. Shiomi, in proceedings of KAON 2016 conference, *J. Phys. Conf. Ser.* **800** (2017) no.1 012022.

PoS(BEAUTY2018)028